Article

Sub-23 nm Particle Emissions from China-6 GDI Vehicle: Impacts of Drive Cycle and Ambient Temperature

Dongdong Guo [1,2], Yunshan Ge [1], Xin Wang [1,*], Haixu Liu [3], Sheng Su [4], Chunbo Li [3] and Tinghong Tao [3]

[1] National Laboratory of Auto Performance and Emission Test, Beijing Institute of Technology, Beijing 100081, China; 7520170034@bit.edu.cn (D.G.); geyunshan@bit.edu.cn (Y.G.)
[2] Beijing Vehicle Emissions Management Center, Beijing 100176, China
[3] Corning Incorporated, Shanghai 201206, China; liuh8@corning.com (H.L.); LiCB@corning.com (C.L.); TaoT@Corning.com (T.T.)
[4] Xiamen Environment Protection Vehicle Emission Control Technology Center, Xiamen 361023, China; sheng.su@vetc.org.cn
[*] Correspondence: xin.wang@bit.edu.cn; Tel.: +86-10-68912035

Abstract: Both the EU and China are evaluating the feasibility of lowering the detection limit of particle number (PN) measurement to 10 nm in future legislations, making it necessary to better understand the sub-23 nm particle emission characteristics from state-of-the-art vehicles. In this study, solid PN emissions with a diameter larger than 10 nm and 23 nm (known as SPN10 and SPN23) were compared over the WLTC, RTS95, and a so-called "worst-case" real driving emission (RDE) cycle (highly dynamic/0 °C) using two certification-level particle number counters (PNCs) employing evaporation tube (ET) and catalytic stripper (CS) as volatile particle remover (VPR). The results show that SPN10 emissions were 31.7%, 27.8%, and 15.2% higher than SPN23 over the WLTC, RTS95, and laboratory RDE cycles. Sub-23 nm particles were almost not identified within the engine cold-start phase and tended to be a hot-running pollutant favored by aggressive driving styles (frequent accelerations and high engine loads), fuel-cut during decelerations, and long idles. Lower testing temperature delayed the light-off of catalyst and, therefore, significantly reduced the formation of sub-23 nm particles within the engine warm-up stage. Lowering the detection limit to 10 nm is deemed to provide more public health protection since it will guide manufacturers to pay more attention to vehicle hot-running emissions.

Keywords: gasoline direct injection (GDI); particulate emission; sub-23 nm particles; real driving emission (RDE)

1. Introduction

Sub-23 nm particles are classified as exhaust particulate matter with a geometric mean diameter (GMD) smaller than 23 nm. They were previously assumed to be only volatile-containing and therefore are currently not considered in the particle number (PN) legislations, given their high measurement sensitivity to counter configurations and unsatisfied result reproducibility [1]. However, an increasing number of recent publications pointed out that the prevalence of sub-23 nm particles in the exhaust and their volatile, as well as solid nature [2–4], pose even stronger harms to human health than the legislated due to larger surface/volume ratio and higher reactivity [5–7]. Along with the commercialization of advanced combustion concepts, emission reduction technologies, and renewable fuels, sub-23 nm particles in the total particle number (TPN) could further climb [8–11].

Driven by the ever-tightening PN legislations and the current focus on 23 nm and larger particles, the wide penetration of diesel particulate filters (DPF) in the market has largely relieved the sub-23 nm concern related to diesel engines. By contrast, it is reported that the PN concentrations from petrol vehicles not equipped with a gasoline

particulate filter (GPF) could exceed DPF-equipped diesel by an order of magnitude with a considerable portion being sub-23 nm [4,12,13].

Many studies have investigated the source and formation mechanisms of sub-23 nm particles from petrol vehicles, but a consensus is yet to be reached. From a traditional point of view, sub-23 nm particles are hydrocarbons that originated from in-cylinder combustion. Giechaskiel et al. summarized that in an overall fuel-rich chamber, fuel and lubricant molecules might pyrolyze into primary soot particles; these particles were in a gas phase and agglomerated. Although most of the primary and agglomerated particles would be oxidized in the combustion process, the small portion that escaped could adsorb non-volatile components like metal or become sub-23 nm particles via self-nucleation once the temperature rapidly dropped as the piston moved downward [3].

Barone et al. observed a dwindling mean diameter of particles from 20–25 nm with normal fuel injection to 10–15 nm with postponed injection on a 2.0-L gasoline direct-injection (GDI) engine using a transmission electron microscope (TEM), better air-fuel blending with reduced fuel impingement were thought the underlying reasons [14]. Similarly, Leach et al. noticed that whether an exhaust recirculation was involved or not, retarding the ignition timing would result in a sharp increase in sub-23 nm particles. Leach et al. also attributed the increased sub-23 nm particle number to the shrinkage in flame size as the engine boosting level was raised [5].

At the chassis level, Saffaripour et al. scrutinized the particle samples from a GDI vehicle collected over the FTP75 and US06 drive cycles. Under a TEM, a fraction of semi-volatile materials was identified, which was thought to be the incomplete resultants of GPF regeneration. Besides, solid particles in nuclei mode were found prevalently distributed downstream of the GPF in US06 testing, which might originate from the in-cylinder combustion or the partial oxidation of the soot particles detached from the inner surfaces of the exhaust system [15].

Di Iorio emphasized that port fuel injection (PFI) petrol engines were also important in terms of sub-23 nm particle emission control as in PFI engines, particles were mainly formed in a small region across the intake valves because, in this locally fuel-rich zone, fuel atomization became difficult so that diffusion combustion replaced premixed combustion [16]. The presence of high-concentration sub-23 nm particles with almost unchanged particulate mass (PM) also indicated the high content of volatile materials [17].

In addition to combustion sources, some other studies confirmed the link between metal-containing sub-23 nm particles and engine fuel-cut. In both laboratory and on-road tests, Ronkko et al. concluded that about 20 to 30 percent of the exhaust particles with a diameter larger than 3 nm were related to vehicle deceleration and engine braking. These particles were non-volatile and composed of lubricant elements such as Ca, P, and Zn. Moreover, volatile particles in nuclei mode were found to be the products of self-nucleation during the cooling down of engine exhaust, while the solid cores of non-volatile particles were assumed combustion-derived [18].

Karjalainen et al. observed the vast amount of fine particle emissions during vehicle deceleration and engine braking in laboratory and on-road tests as well. These particles traversed a broad size range from 10 to 200 nm. The detected Ca, P, and Zn suggested these particles were plausibly lubricant oil-originated. Besides, it is also inferred that a fraction of 10–20 nm particles were formed under high temperatures as they were charged and amorphous in structure [12].

More metal elements, including Mg, Fe, S, Sn, and W, were identified in the Energy Dispersive X-ray-based research conducted by Liati et al. [19]. Unlike hydrocarbons and soot comprised larger exhaust particles, ash occupied at least an equivalent portion to soot in the nanoparticles, possibly because the concentration of ash in the exhaust was too low to agglomerate, which was opposite to the results of Qin et al., who found blending lubricant oil into petrol mainly increased the number of accumulation mode particles [20]. Si was also detected in some sub-23 nm samples. Liati et al. were inclined to conclude that washcoat components dropped from the three-way catalyst (TWC), but Giechaskiel et al.

speculated that it belonged to the silicon adaptors connecting tailpipe and dilution tunnel particularly in the high and ex-high stages of the World Harmonized Light-duty Test cycle (WLTC) when the exhaust temperature was hot [21].

There is also research suggesting that sub-23 nm particles could be a result of a deficiency in current volatile particle remover (VPR) designs. Zheng and Johnson et al. noticed that some of the sub-23 nm particles counted by PN instruments might be influenced by the reactions between sulfuric acid and hydrocarbon droplets downstream the VPR [22–25]. This was in strong agreement with the experimental observations of Amanatidis and Otsuki et al. [26,27]. Zheng and Johnson pointed out that another part of the 3–10 nm particles could have arisen from the re-nucleation of exhaust-borne semi-volatile materials [22–25], supported by the test results of Giechaskiel and Yamada et al. [4,28].

Considering that both the EU and China are evaluating the feasibility of legislating exhaust particles down to 10 nm, several recent research activities focused on the effectiveness of after-treatment devices on removing sub-23 nm particles. Whelan et al. reported that a TWC managed to eliminate roughly 60% of engine-out particles with a diameter range from 5 to 10 nm at part load. However, this performance quickly deteriorated to 6% at higher loads [29]. As recommended by Bogarra et al., who noticed the desirable removal efficiency of TWC towards 5–10 nm particles as well, complementary devices shall be enrolled to meet more stringent future legislations [30].

Dorscheidt et al. tested the particle concentrations and their size distributions over the entire engine map n a direct-injection petrol engine, and the filtration efficiency of GPF towards sub-23 nm particles increased with the engine speed and load but showed an opposite tendency towards larger particles (up to 200 nm). The filtration efficiency was also promoted with heavier soot and ash load [31]. Baek et al. justified metal-foam GPF as another technical route for reducing sub-23 nm particles apart from wall-flow GPF [32]. It is also noticed that the filtration mechanisms in cold-start, high-speed driving, and harsh accelerations were quite different from other operating conditions. The authors attributed these differences to the complicated interactions between the oxidation and storage of volatile species and solid particles.

Samaras et al. assessed the sub-23 nm particle emissions from state-of-the-art vehicles using a down-to-10 nm measurement system. For the petrol vehicles without GPF, the number concentrations of sub-23 nm particles exceeded those of particles above 23 nm. Regarding GPF-equipped vehicles, lowering the threshold from 23 to 10 nm caused an increase of 44% in number, suggesting a GPF could be more effective in blocking sub-23 nm particles as a result of the diffusion collection mechanism [2].

Above all, the sources of sub-23 nm particles from petrol vehicles could be summarized as in-cylinder combustion, lubricant oil, and possible artefact due to nucleation downstream of the VPR. Both TWC and GPF have been shown useful for the removal of sub-23 nm particles from the exhaust. However, given the real driving emission (RDE) requirements started from Euro-6d and China-6, sub-23 nm particles shall be tested with not only regulatory cycles, but also more realistic speed profiles, and the impacts of more boundary conditions shall be examined.

In this study, a conventional petrol vehicle powered by a turbocharged 1.2-L direct-injection engine without a particulate filter mounted was employed as the test vehicle; its solid particle number above 10 nm (SPN10) and 23 nm (SPN23) emissions were compared over three test cycles, namely a type-approval WLTC (23 °C), an aggressive cycle RTS95 (23 °C), and a so-called "worst-case" RDE cycle for in-use compliance (0 °C). The effects of driving activities and ambient temperature on the exhaust emissions of sub-23 nm particles were discussed.

2. Materials and Methods

2.1. Test System, Vehicle, and Fuel

All the tests were performed at a certification level test cell for data quality assurance purposes. Figure 1 depicts the arrangement of the test facilities, and the key information about the test instruments are specified in Table 1.
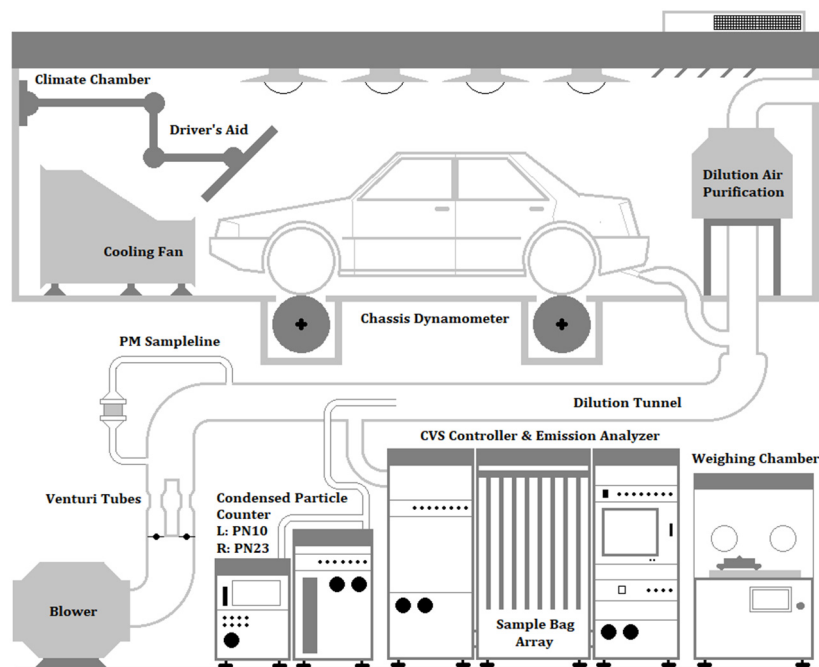
Figure 1. Systematic sketch of the test facilities.

Table 1. Specifications of the testing instruments.

Instrument	Make/Model	Details
Climate chamber	Imtech EC45192327	Temperature: −10–40 °C with control accuracy of ±1 °C Relative humidity: 5–90% RH with control accuracy of ±5% RH
Chassis dynamometer	AVL RPL 1220	48'roller-wheels, four-wheel drive compatible, maximum speed up to 200 km/h with control accuracy of ±1%; inertial weight: 454–5400 kg; parasitic loss: <5 N; traction control: 3% FS
Constant volume sampler	AVL CVS i60LD	Full-flow CVS with critical Venturi tube controlled diluted exhaust flow rate: 3–18 m^3/min
Emission analyzer	AVL AMA i60	THC/CH$_4$: 0–20,000 ppmC$_3$, heated flame ionization detector (FID). noise: ≤0.5% full scale (FS); linearity: ≤1% FS or 2% measured value, whichever is smaller; reproducibility: ≤0.5% FS
		NOx: 0–1000 ppm, chemi-luminesence detector (CLD). noise: ≤1% full scale (FS); linearity: ≤1% FS or 2% measured value, whichever is smaller; reproducibility: ≤0.5% FS
		CO$_2$: 0–20%, infrared detector; CO: 0–5000 ppm, infrared detector. noise: ≤1% full scale (FS); linearity: ≤1% FS or 2% measured value, whichever is smaller; reproducibility: ≤0.5% FS
		N$_2$O: 0–100 ppm, continuous-wave quantum cascade LASER spectrometric detector. noise: ≤0.3 % full scale (FS); linearity: ≤1% FS or 2% measured value, whichever is smaller; reproducibility: ≤0.5% FS
PM sampler	AVL PSS i60	Sample flow rate: 95 L/min; 47 mm stainless steel holder; flow rate control: ±1.5%
PN measurement	AVL 489 APC	Condensation particle counter (CPC); cut-off efficiency: 50% at 23 nm
PN measurement	HORIBA MEXA-2310SPCS	Condensation particle counter (CPC); cut-off efficiency: 60% at 10 nm

To compare the SPN10 and SPN23 emissions from the test vehicle. Two PMP-compliant particle number counters (PNCs) were employed in this research. SPN23 was measured by

a classic AVL 489 system, which adopted a two-stage dilution system with an evaporation tube (ET) as the volatile particle remover (VPR). SPN10 was quantified by a HORIBA MEXA-2300SPCS prototype system, utilizing a standard two-stage dilution system with a catalytic stripper (CS) as the VPR. The sampling probes of the two PN counters were circumferentially placed inside the dilution tunnel near the center of the cross-section. The flow rate of the constant volume sampler (CVS) was set to 16.5 m^3/min as per the engine displacement of the test vehicle. Both two PN instruments used calibrated butanol CPC built under the guidance of the ongoing regulation as the core; hence the results of the two instruments were considered comparable.

The test vehicle was a 2019 model year sedan conforming to China-6b standard. This vehicle was manufactured and registered in January 2020 and has run 34,780 km when tested. No abusivedriving, wrong fueling, improper maintenance, or repair was recorded. Before each test, the tire pressure was checked and adjusted to 230 kPa as recommended.

RON 95 petrol compliant with China-6 base fuel was fed to the test vehicle. Before testing, the fuel tank was drained and flushed with the test fuel three times. The fuel tank was topped up to finish all the planned tests to isolate the possible influences upon results due to refueling.

2.2. Test Plan and Repeatability

Three drive cycles were tested in this study, namely a room-temperature (23 °C) WLTC representing the standard type-approval condition, a 23 °C RTS95 cycle reflecting one of the harshest driving styles in the laboratory, and a laboratory RDE cycle modified from an aggressive RDE trip exactly fulfill the dynamic validation. The laboratory RDE cycle was designed to aim at gaining the worst emission performance without entering the extended boundary condition as defined in the RDE regulation, also known as "worst-case RDE", particularly in the industry. For this purpose, the testing temperature was set to low-temperature (0 °C), and the driving dynamics were adjusted as extreme as possible. The speed profiles of the three drive cycles were illustrated together with the emission results when discussed.

Three repeats of WLTC for the test vehicle were first performed in a row, and then RTS95 and laboratory RDE. The WLTC tests were also performed to secure the technical status of this test vehicle was suitable for this comparative research. The test results were depicted in Table 2 in context to the regulatory limit values of China-6b. All the regulated emissions were always more than 50% lower than the limits, and except for PM and N2O, the emission factors of which were too low, resulting in much higher variations among repeats, the standard deviations of the rest pollutants were smaller than 15% and absolute differences between any two repeats were almost negligible.

Table 2. Results of three repeated WLTC tests.

		Repeat #1	Repeat #2	Repeat #3	Average	Standard Deviation	Deviation In %	Limit Value
THC	(mg/km)	13.2	13.3	13.2	13.23	0.06	0.44	50
CO	(mg/km)	129.9	129.0	119.6	126.19	5.72	4.53	500
NOx	(mg/km)	6.2	5.2	6.9	6.08	0.86	14.06	35
CO_2	(g/km)	145.33	141.44	140.15	142.31	2.70	1.90	N/A
CH_4	(mg/km)	1.2	1.1	1.2	1.17	0.05	3.98	N/A
NMHC	(mg/km)	12.1	12.2	12.0	12.10	0.10	0.84	35
N_2O	(mg/km)	0.4	0.4	0.7	0.53	0.16	29.06	20
PM	(mg/km)	0.09	0.21	0.11	0.14	0.07	48.86	3.0
SPN23	(#/km)	2.79×10^{11}	3.05×10^{11}	2.81×10^{11}	2.89×10^{11}	1.43×10^{10}	4.96	6.0×10^{11}
FE	(L/100 km)	6.19	6.02	5.97	6.06	0.12	1.90	N/A

In accordance with the regulation and as a required measure for result quality assurance, before each test, the test vehicle was refilled and ran the testing drive cycle once as a

pre-conditioning drive. After the pre-conditioning drive, the test vehicle was placed in the soaking room for 12–20 h of soaking, and the temperature of the room was adjusted to the testing temperature of the upcoming test, namely 23 °C for the WLTC and RTS95 and 0 °C for the laboratory RDE.

3. Results and Discussion

3.1. PN10 vs. SPN23 over Various Drive Cycles

As introduced in the methodology section, the SPN23 and SPN10 emissions from this GDI test vehicle were measured simultaneously using two PNCs. The modal data of SPN23 and SPN10 emissions over one of the three WLTC repeats are plotted in Figure 2, while in Table 3 the PN results of the entire drive cycle and its four stages were compared.
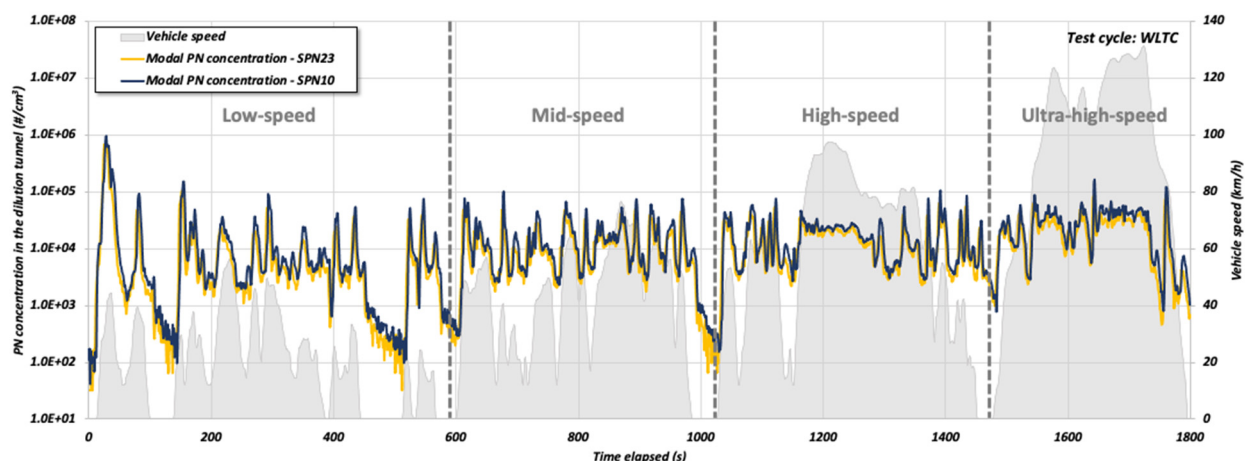

Figure 2. Comparison between SPN23 and SPN10 emissions over the WLTC.

Table 3. Distance-based PN results of SPN23 and SPN10 over the WLTC.

		WLTC	Low	Mid	High	Ultra-High
SPN23	(#/km)	3.05×10^{11}	8.36×10^{11}	2.66×10^{11}	2.18×10^{11}	2.16×10^{11}
SPN10	(#/km)	4.02×10^{11}	1.12×10^{12}	3.48×10^{11}	2.74×10^{11}	2.90×10^{11}
Increment	%	31.7	34.0	30.8	25.6	34.5

It can be seen in Figure 2 that, apart from the initial 100 s, the SPN10 concentrations were always higher than the SPN23 concentrations. As tabulated in Table 3, the distance-based SPN10 emission factor is 31.7% higher than SPN23 over the entire WLTC, meaning that about 24% of the PN emissions from the test vehicle were sub-23 nm particles. This percentage strongly agrees with prior studies [8]. In comparison to the China-6b limit of 6.0×10^{11} #/km, the SPN10 from the test vehicle is roughly 2/3 of the regulatory limit, indicating that under WLTC driving conditions, the state-of-the-art direct-injection technology would be compliant to the forthcoming requirement without accounting for a reasonable engineering margin regarding the manufacturing errors across the mass production models.

The difference between SPN23 and SPN10 emissions in the cold-start and warm-up stages were less pronounced than that in the rest of the test cycle. This feature suggested that the engine was inclined to emit a greater amount of smaller particles once warmed up, or in other words, sub-23 nm particles will become a concern after the light-off of the after-treatment system. This finding is largely in agreement with Yamada et al. [28]. On the one hand, the cold operation produced more large particles as the relatively low temperature in chambers worsened fuel atomization and the following air-fuel blending process. On the other hand, given that the cylinder temperature was also low and the TWC had not been lit off at this stage, the reaction rates of the oxidation reactions consuming formed particles

remained low, which significantly stalled the conversion from agglomerates to the nucleus. Both factors could result in particle emissions with larger diameters.

Among the four stages, the increments with a lower detection limit down to 10 nm of mid- and high-speed stages are below the WLTC average, while both low- and ultra-high-speed stages show slightly larger increments. It is noticeable in Figure 2 that the low-speed stage of WLTC with the most frequent accelerations; meanwhile, the engine load of the test vehicle is the highest in the ultra-high-speed stage, particularly during the few harsh accelerations. From an engine combustion viewpoint, sub-23 nm particles originated from the shrinkage in flame size as cylinder pressure increases could explain this phenomenon [33,34]. This result is also supported by Karjalainen et al. [12], who observed that in both laboratory and real-world tests, bimodal PN size distributions with one peak around 20–30 nm were detected during acceleration events.

Another detail to notice is the obvious increase in the sub-23 nm portion during long idle events. This fact partially underlays the higher sub-23 nm portion of the mid-speed stage compared to high-speed. Apart from the idle in between the high-speed and ultra-high-speed stages, the increments with the lower detection limit down to 10 nm within the four relatively long idle are calculated, which are 69.8%, 66.0%, 44.5%, and 73.6% for the periods of 103–144 s, 457–509 s, 593–605 s, and 1000–1030 s respectively. The larger portion of sub-23 nm particles during long idles may be a successive consequence of the decelerations before. Engine control units enrolled fuel-cut strategies during deceleration, fuel vapor released from the oil film on the cylinder wall via mass transfer, and lubricant oil vapor most likely transported to the combustion chamber through crankcase ventilation system could be converted into sub-23 nm particles improves fuel economy, [18]. Due to the very low intake flow rates, the release process of the sub-23 nm particles formed during deceleration could plausibly be extended until the end of the following long idle. Similar results were also reported by Karjalainen et al. and Rönkkö et al. [12,18]. Exhaust temperature dropped by a few hundred degrees once the engine entered idle could also cool down some semi-volatile materials and cause an increase in sub-23 nm particles. Fuel-cut induced a reduction of tailpipe PN concentration, enhancing the transfer of the particles previously adsorbed on the inner surface of the exhaust system to the exhaust stream as the concentration difference became larger.

Besides, as depicted in Figure 2, the readings of the SPN23 were with more variations at low PN concentration level around 1×10^2 to 1×10^3 #/cm^3. This phenomenon is also deemed as evident for the better removal efficiency of a catalytic stripper as an exhaust-borne volatile materials remover because Giechaskiel et al. pointed out that the organic carbon proportion of petrol particles increased as engine load decreased [3]. A similar tendency was observed in the RTS95 testing as well as illustrated in Figure 3.
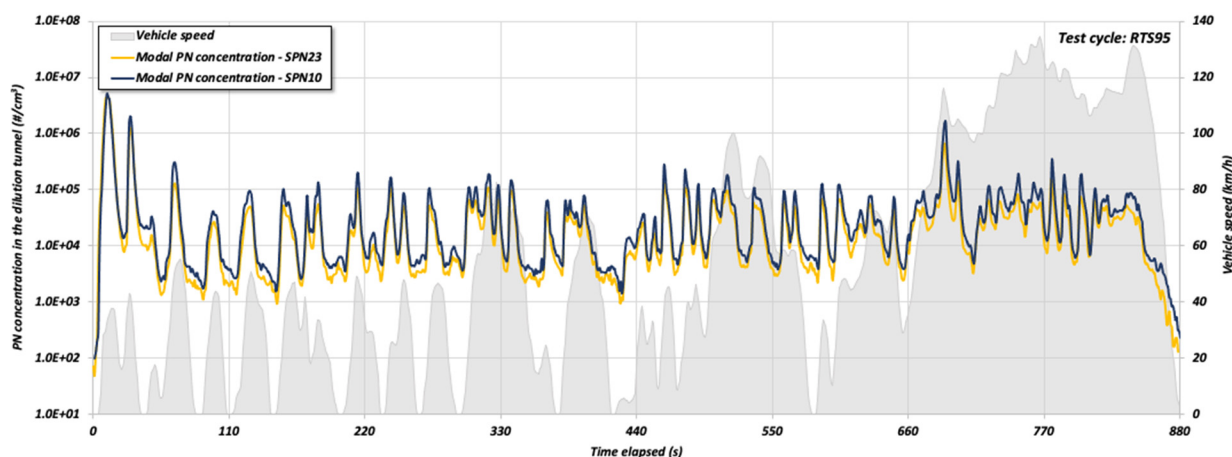

Figure 3. Comparison between SPN23 and SPN10 emissions over the RTS95.

Figure 3 represents the SPN10 and SPN23 emissions of the test vehicle over the RTS95 cycle. As reported in the methodology, the RTS95 cycle is widely adopted by the industry because of its aggressive driving style and good indication for RDE results. Its aggressive feature can also be seen from the results. The distance-based emission factors of SPN10 and SPN23 emissions over the RTS95 are 1.41×10^{12} and 1.10×10^{12} #/km, respectively, which were approximately two times higher than the WLTC results.

In the RTS95 test, SPN10 is only 27.8% larger than SPN23 emissions, or sub-23 nm particles accounted for about 22% of total PN emissions identified. This percentage is in agreement with the 24–87% increase for port fuel injection vehicles, with the 10 nm being the lower detection limit reported by Giechaskiel et al. [21], but smaller than expected (even smaller than 31.7% of the WLTC) given the highly dynamic feature of the RTS95. Engine cold-start and the following 40 s of warm-up may explain this phenomenon. It can be seen in Figure 3 that within this short period, almost all the exhaust particles were above 23 nm; meanwhile, the PN concentrations were roughly one to two orders of magnitude higher than the rest spikes. Since the RTS95 cycle only lasts for about 900 s, cold-start emissions will have stronger impact on the cycle results. The increments with lower detection limits down to 10 nm of 41–300 s, 301–595 s, and 595–880 s of the RTS95 cycle are 79.9%, 57.5%, and 184.9%. These numbers highlight that frequent acceleration, in particular when the engine load has been at a high level, will exacerbate the problem of sub-23 nm particle emissions.

In addition, by comparing the results over the WLTC and RTS95, it can be inferred that the formation of sub-23 nm particles is favored by higher temperatures in combustion chambers and after-treatment systems; hence, more dynamic driving styles will be more challenging for future SPN10 emission compliance.

Figure 4 illustrates the modal data of SPN10 and SPN23 emissions over the laboratory RDE cycle. As explained in the methodology section, this laboratory RDE cycle was modified from a valid real-world trip with the first 300 s of drive replaced by the first 300 s of RTS95, attempting to gain the worst emission performance within the regulatory boundary. Cycle-based and the results divided into urban, rural, and highway phases are given in Table 4. A comparison between the laboratory RDE results with the WLTC and RTS95 shows that on a cycle average, for both SPN10 and SPN23, the WLTC data will underestimate 75% of the worst-case RDE emissions. Although the laboratory RDE and RTS95 were tested at 0 °C and 23 °C, respectively, the RTS95 results were indicative of RDE performance. The increment between SPN10 and SPN23 over the laboratory RDE cycle is 15.2%, which is narrower than the RTS95 and WLTC. A non-negligible reason is the lower testing temperature, significantly prohibiting the formation of sub-23 nm at the very beginning of the test. This factor will be discussed in detail in the following section. Once the engine warmed up, in Figure 4, the gap between SPN10 and SPN23 emissions can be clearly identified. Besides, the more pronounced increment in sub-23 nm particles during long idles is also observed at low temperatures in Figure 4.
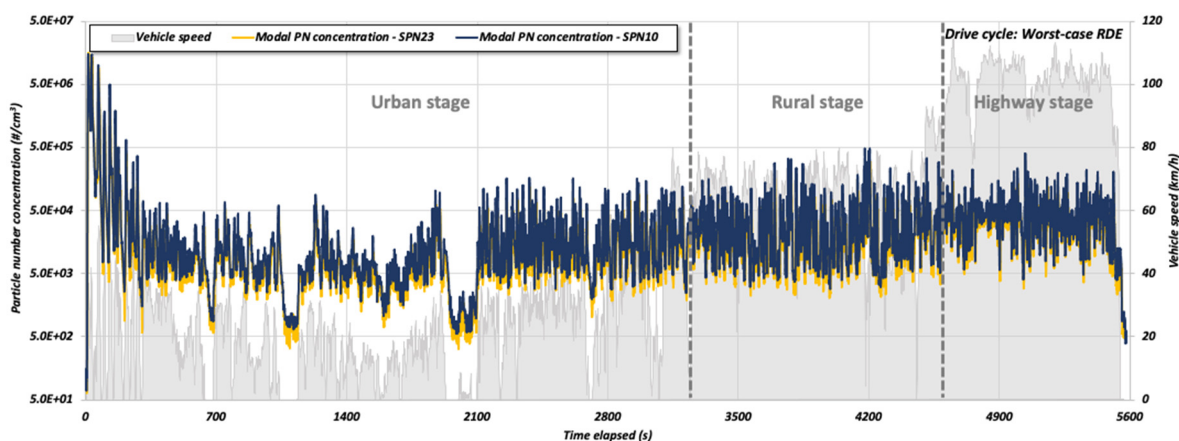

Figure 4. Comparison between SPN23 and SPN10 emissions over a worst-case RDE cycle.

Table 4. Distance-based PN results of SPN23 and SPN10 over the laboratory RDE cycle.

	Duration (s)	Distance (km)	SPN10 (#/km)	SPN23 (#/km)	Increment (%)
Urban	3062	26.09	3.45×10^{12}	3.14×10^{12}	10.0
Rural	1531	17.67	8.90×10^{11}	6.35×10^{11}	40.1
Highway	1141	26.24	4.88×10^{11}	3.49×10^{11}	40.0
Trip	5581	70.00	1.63×10^{12}	1.41×10^{12}	15.2

Unlike the quite low increment in the urban stage, the differences between SPN10 and SPN23 emissions during rural and highway operations are around 40%, markedly larger than any other stage of the WLTC. Hence, it will be helpful that more calibration work shall be paid to these two conditions if the future regulations decide to employ SPN10 as the new criteria. As mentioned above, according to the modal data over the three test cycles, sub-23 nm particles tend to be a hot-running pollutant. To solve this issue, employing GPF could be a solution, as many previous studies have reported the very high filtration efficiency of GPFs in removing tiny particles via thermal diffusion [35,36]. However, it is still worth noting that though the increment in the urban stage of the laboratory RDE cycle was only 10%, the distance-based SPN10 emissions have been 3.45×10^{12} #/km. From a public welfare perspective, it is necessary to set more stringent requirements to cap nanoparticle emissions in urban areas to reduce human exposure and related chronic health damages.
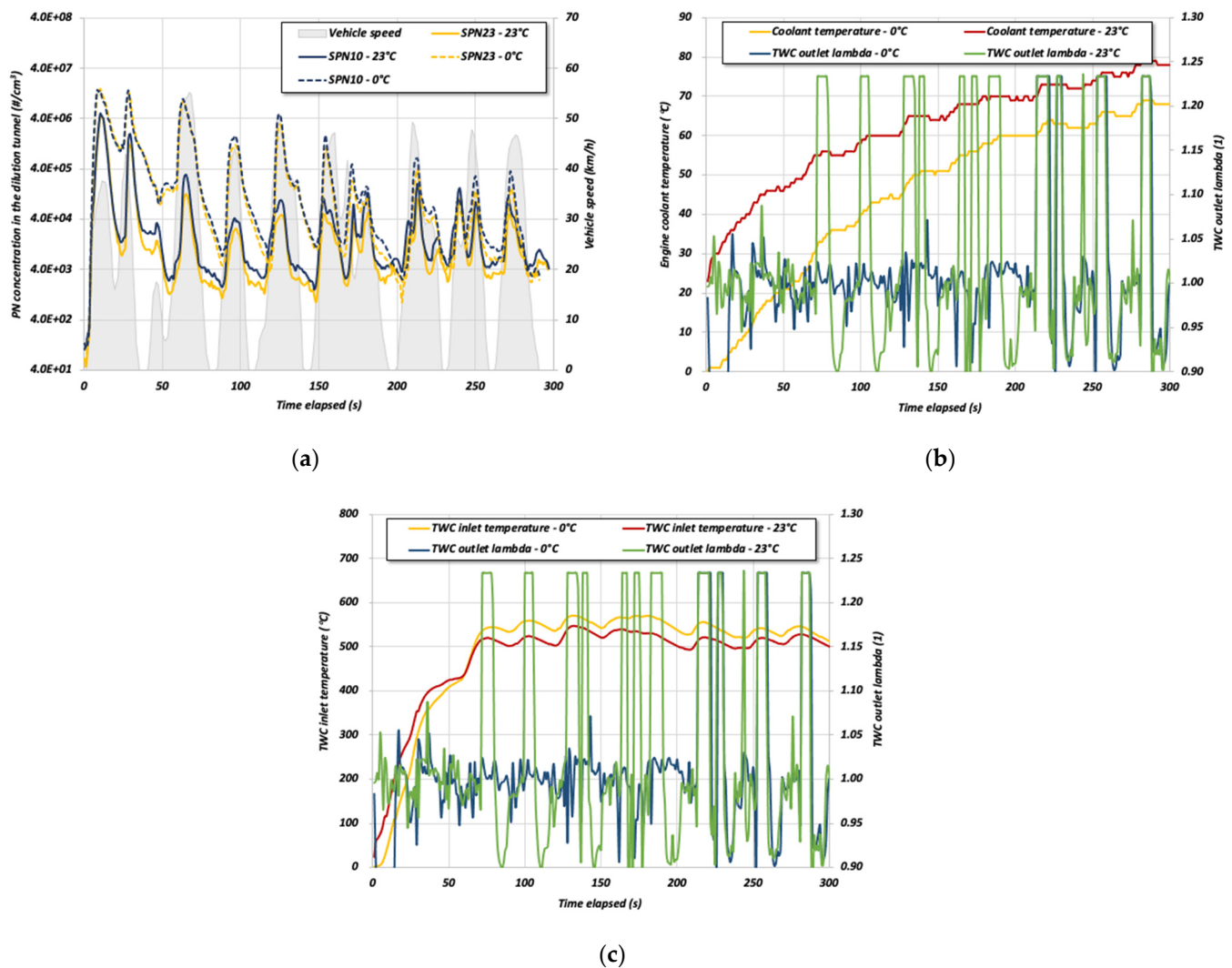
3.2. Impacts of Ambient Temperature

As introduced in the methodology section, the first 300 s of the laboratory RDE cycle are identical to RTS95, enabling a comparison between the two tests to see the impacts of ambient temperature on SPN10 and SPN23 emissions. Figure 5a plots the instantaneous SPN10 and SPN23 concentrations measured at 0 and 23 °C together. Meanwhile, the real-time catalyst temperature and excess air ratio (lambda) data acquired through the OBD port is also provided.

It can be seen in Figure 5 that the first, as well as the highest PN spikes, appeared when the test vehicle started and began to accelerate at both testing temperatures. However, in the 0 °C cases, the PN spike was approximately 3-fold higher, which was a consequence of the further enriched air-fuel mixtures under the low-temperature condition as compensation for worsened fuel atomization, which could be seen in Figure 5b.

At both 0 and 23 °C, SPN10 and SPN23 were very close at the initial stage of testing, suggesting cold-start particles were dominated by large ones. This observation can also be explained by fuel enrichment, poor atomization of fuel droplets, and combustion incompleteness in chilled combustion chambers.

Interestingly, as shown in Figure 5a, differences in particle size can be seen in the next ~1 min of testing. At room temperature, the gap between SPN10 and SPN23 baseline widens during the second acceleration (PN spike), and SPN10 becomes obviously higher than SPN23 after the fourth acceleration. However, in the 0 °C test, the "separation timing" for SPN10 diverging from SPN23 is much delayed than in the room temperature case. The gaps between SPN10 and SPN23 can only be identified after the sixth acceleration. This difference is backboned by the faster warming-up as depicted in Figure 5b, which allows the earlier introduction of the fuel-cut strategy at room temperature. It is also illustrated in Figure 5b that at both testing temperatures, the appearance of SPN10 and SPN23 "separation" accurately accords with the maneuvering of fuel-cut during decelerations (engine braking) indicated by OBD lambda values jump to above 1.2, confirming the tight correlation between the major release of sub-23 nm particles and fuel-cut. This tendency also agrees well with some previous studies reported [4,17].

(**a**)

(**b**)

(**c**)

Figure 5. SPN23 and SPN10 comparison performed at 0 and 23 °C over the initial 300 s of RTS95. (**a**) Modal data of SPN23 and SPN10; (**b**) Coolant temperature and lambda for 0 and 23 °C; (**c**) TWC inlet temperature and lambda for 0 and 23 °C.

In Figure 5c, TWC inlet temperature is plotted versus TWC outlet lambda as a function of time. In the first 60 s after starting the test, the TWC inlet temperature in the room temperature case is various degrees higher than that at 0 °C. The crossover happens at 60 s near 420 °C. Shortly after that timing, the fuel cut is called in the room temperature test. For this reason, the TWC inlet temperature in the 0 °C cases is always higher than that in the room temperature test until the fuel cut is also maneuvered later. Once the fuel cut strategy is introduced in both cases with the TWC inlet temperature largely exceeding 500 °C, the temperature difference becomes narrowed after 250 s. It is reasonable to mark sub-23 nm particles from direct-injection petrol engines as a hot-running pollutant because of its close link with fuel-cut, while fuel-cut only becomes available with both engine coolant and TWC meeting calibration thresholds when combining the observations in Figure 5b,c.

Based on the above findings, it will be a good move if the upcoming regulations in the EU and China set the threshold down to 10 nm since this new requirement will guide the manufacturers to pay more attention to hot-running emissions in addition to cold-starts. Together with the ever-tightening RDE requirements, the down-to-ten program will benefit the reduction of real-world driving emissions.

4. Conclusions and Implications

To understand the sub-23 nm emission characteristics of a representative China-6b compliant GDI passenger car, WLTC and RTS95 tests and laboratory RDE tests were performed at room and low temperature, respectively. Second-by-second SPN10 and SPN23 emissions were measured using certification level PNCs employing ET and CS as VPR. The following conclusions are made.

(1) On a cycle average, SPN10 exceeded SPN23 emissions by 31.7%, 27.8%, and 15.2% over the WLTC, RTS95, and laboratory RDE. State-of-the-art engine technology has been able to fulfill an SPN10 limit of 6.0×10^{11} #/km, but a reasonable engineering margin regarding mass production errors shall be further concerned.

(2) More aggressive driving behaviors, such as frequent accelerations, particularly at high engine loads, increased the concentrations of sub-23 nm particles and their shares in the total PN emissions because sub-23 nm particles tended to be a hot-running pollutant.

(3) Fuel-cut during decelerations and long idles also favored the formation of sub-23 nm particles and resulted in larger discrepancies between SPN10 and SPN23.

(4) Lower ambient temperature prolonged the time for TWC light-off and hence significantly depressed the production of sub-23 nm particles within this period. The SPN10 and SPN23 cruces became more divergent once the activation of TWC, suggesting sub-23 nm could plausibly be linked with TWC oxidation reactions.

Unlike most of the regulated emissions, in the post-Euro-6/China-6 era, SPN10 (if considered as a criterion pollutant) may see higher compliance risk in laboratory tests and RDE sections with higher speeds. Lowering the detection limit from 23 nm to 10 nm is deemed to provide more protection for the public, not only because this move will further tighten the emission limit but also because it drives the manufacturers to pay more attention to hot-running pollutants.

Author Contributions: Conceptualization, X.W., H.L. and D.G.; methodology, D.G., X.W. and S.S.; validation, D.G., Y.G., X.W., H.L. and C.L.; formal analysis, D.G. and X.W.; investigation, D.G., X.W. and H.L.; resources, Y.G., S.S., C.L. and T.T.; data curation, D.G., X.W. and H.L.; writing—original draft preparation, D.G.; writing—review and editing, X.W., Y.G., H.L., C.L. and T.T.; visualization, X.W.; supervision, Y.G. and X.W.; project administration, X.W. and H.L.; funding acquisition, X.W. All authors have read and agreed to the published version of the manuscript.

Institutional Review Board Statement: Not applicable.

Informed Consent Statement: Not applicable.

Data Availability Statement: The data presented in this study are available on request from the corresponding author.

Conflicts of Interest: The authors declare no conflict of interest.

References

1. Baltzopoulou, P.; Melas, A.D.; Vlachos, N.; Deloglou, D.; Papaioannou, E.; Konstandopoulos, A.G. Solid Nucleation Mode Engine Exhaust Particles Detection at High Temperatures with an Advanced Half Mini DMA. *SAE Tech. Pap. Ser.* **2020**, *1*, 535–542.
2. Samaras, Z.C.; Andersson, J.; Bergmann, A.; Hausberger, S.; Toumasatos, Z.; Keskinen, J.; Haisch, C.; Kontses, A.; Ntziachristos, L.D.; Landl, L.; et al. Measuring Automotive Exhaust Particles down to 10 nm. *SAE Tech. Pap.* **2020**, *2017*, 1–12. [CrossRef]
3. Giechaskiel, B.; Manfredi, U.; Martini, G. Engine Exhaust Solid Sub-23 nm Particles: I. Literature Survey. *SAE Int. J. Fuels Lubr.* **2014**, *7*, 950–964. [CrossRef]
4. Giechaskiel, B.; Vanhanen, J.; Väkevä, M.; Martini, G. Investigation of Vehicle Exhaust Sub-23 nm Particle Emissions. *Aerosol Sci. Technol.* **2017**, *51*, 626–641. [CrossRef]
5. Donaldson, K.; Li, X.Y.; MacNee, W. Ultrafine (Nanometre) Particle Mediated Lung Injury. *J. Aerosol Sci.* **1998**, *29*, 553–560. [CrossRef]

6. Gidney, J.T.; Twigg, M.V.; Kittelson, D.B. Effect of Organometallic Fuel Additives on Nanoparticle Emissions from a Gasoline Passenger Car. *Environ. Sci. Technol.* **2010**, *44*, 2562–2569. [CrossRef]

7. Oberd Örster, G. Significance of Particle Parameters in the Evaluation of Exposure-Dose Response Relationships of Inhaled Particles. *Part. Sci. Technol.* **1996**, *14*, 135–151. [CrossRef]

8. Leach, F.; Lewis, A.; Akehurst, S.; Turner, J.; Richardson, D. Sub-23 nm Particulate Emissions from a Highly Boosted GDI Engine. *SAE Tech. Pap.* **2019**, *24*, 153.

9. Maier, T.; Härtl, M.; Jacob, E.; Wachtmeister, G. Dimethyl Carbonate (DMC) and Methyl Formate (MeFo): Emission Characteristics of Novel, Clean and Potentially CO2-Neutral Fuels Including PMP and Sub-23 nm Nanoparticle-Emission Characteristics on a Spark-Ignition DI-Engine. *Fuel* **2019**, *256*, 115925. [CrossRef]

10. Singh, R.; Han, T.; Fatouraie, M.; Mansfield, A.; Wooldridge, M.; Boehman, A. Influence of Fuel Injection Strategies on Efficiency and Particulate Emissions of Gasoline and Ethanol Blends in a Turbocharged Multi-Cylinder Direct Injection Engine. *Int. J. Engine Res.* **2021**, *22*, 152–164. [CrossRef]

11. Toumasatos, Z.; Kontses, A.; Doulgeris, S.; Samaras, Z.; Ntziachristos, L. Particle Emissions Measurements on CNG Vehicles Focusing on Sub-23nm. *Aerosol Sci. Technol.* **2020**, *55*, 182–193. [CrossRef]

12. Karjalainen, P.; Pirjola, L.; Heikkilä, J.; Lähde, T.; Tzamkiozis, T.; Ntziachristos, L.; Keskinen, J.; Rönkkö, T. Exhaust Particles of Modern Gasoline Vehicles: A Laboratory and an On-Road Study. *Atmos. Environ.* **2014**, *97*, 262–270. [CrossRef]

13. Kim, J.; Choi, K.; Myung, C.L.; Lee, Y.; Park, S. Comparative Investigation of Regulated Emissions and Nano-Particle Characteristics of Light Duty Vehicles Using Various Fuels for the FTP-75 and the NEDC Mode. *Fuel* **2013**, *106*, 335–343. [CrossRef]

14. Barone, T.L.; Storey, J.M.E.; Youngquist, A.D.; Szybist, J.P. An Analysis of Direct-Injection Spark-Ignition (DISI) Soot Morphology. *Atmos. Environ.* **2012**, *49*, 268–274. [CrossRef]

15. Saffaripour, M.; Chan, T.W.; Liu, F.; Thomson, K.A.; Smallwood, G.J.; Kubsh, J.; Brezny, R. Effect of Drive Cycle and Gasoline Particulate Filter on the Size and Morphology of Soot Particles Emitted from a Gasoline-Direct-Injection Vehicle. *Environ. Sci. Technol.* **2015**, *49*, 11950–11958. [CrossRef] [PubMed]

16. di Iorio, S.; Catapano, F.; Sementa, P.; Vaglieco, B.M.; Nicol, G.; Sgroi, M.F. Sub-23 nm Particle Emissions from Gasoline Direct Injection Vehicles and Engines: Sampling and Measure. *SAE Tech. Pap.* **2020**, *01*, 396.

17. di Iorio, S.; Catapano, F.; Vaglieco, B.M.; Continillo, G.; Petito, G. Analysis of the Effect of the Sampling Conditions on the sub-23 nm Particles Emitted by a Small Displacement PFI and di SI Engines Fueled with Gasoline, Ethanol and a Blend. *SAE Tech. Pap.* **2019**, *24*, 155.

18. Rönkkö, T.; Pirjola, L.; Ntziachristos, L.; Heikkilä, J.; Karjalainen, P.; Hillamo, R.; Keskinen, J. Vehicle Engines Produce Exhaust Nanoparticles Even When Not Fueled. *Environ. Sci. Technol.* **2014**, *48*, 2043–2050. [CrossRef] [PubMed]

19. Liati, A.; Schreiber, D.; Dasilva, Y.A.R.; Eggenschwiler, P.D. Ultrafine Particle Emissions from Modern Gasoline and Diesel Vehicles: An Electron Microscopic Perspective. *Environ. Pollut.* **2018**, *239*, 661–669. [CrossRef] [PubMed]

20. Qin, J.; Li, X.; Pei, Y. Effects of Combustion Parameters and Lubricating Oil on Particulate Matter Emissions from a Turbo-Charged GDI Engine Fueled with Methanol/Gasoline Blends. *SAE Tech. Pap.* **2014**, *01*, 2841.

21. Giechaskiel, B.; Woodburn, J.; Szczotka, A.; Bielaczyc, P. Particulate Matter (PM) Emissions of Euro 5 and Euro 6 Vehicles Using Systems with Evaporation Tube or Catalytic Stripper and 23 nm or 10 nm Counters. *SAE Tech. Pap.* **2020**, *01*, 2203.

22. Zheng, Z.; Johnson, K.C.; Liu, Z.; Durbin, T.D.; Hu, S.; Huai, T.; Kittelson, D.B.; Jung, H.S. Investigation of Solid Particle Number Measurement: Existence and Nature of Sub-23nm Particles under PMP Methodology. *J. Aerosol Sci.* **2011**, *42*, 883–897. [CrossRef]

23. Zheng, Z.; Durbin, T.D.; Karavalakis, G.; Johnson, K.C.; Chaudhary, A.; Cocker, D.R.; Herner, J.D.; Robertson, W.H.; Huai, T.; Ayala, A.; et al. Nature of Sub-23-Nm Particles Downstream of the European Particle Measurement Programme (PMP)-Compliant System: A Real-Time Data Perspective. *Aerosol Sci. Technol.* **2012**, *46*, 886–896. [CrossRef]

24. Zheng, Z.; Durbin, T.D.; Xue, J.; Johnson, K.C.; Li, Y.; Hu, S.; Huai, T.; Ayala, A.; Kittelson, D.B.; Jung, H.S. Comparison of Particle Mass and Solid Particle Number (SPN) Emissions from a Heavy-Duty Diesel Vehicle under On-Road Driving Conditions and a Standard Testing Cycle. *Environ. Sci. Technol.* **2014**, *48*, 1779–1786. [CrossRef]

25. Johnson, K.C.; Durbin, T.D.; Jung, H.; Chaudhary, A.; Cocker, D.R.; Herner, J.D.; Robertson, W.H.; Huai, T.; Ayala, A.; Kittelson, D. Evaluation of the European PMP Methodologies during On-Road and Chassis Dynamometer Testing for DPF Equipped Heavy-Duty Diesel Vehicles. *Aerosol Sci. Technol.* **2009**, *43*, 962–969. [CrossRef]

26. Amanatidis, S.; Ntziachristos, L.; Karjalainen, P.; Saukko, E.; Simonen, P.; Kuittinen, N.; Aakko-Saksa, P.; Timonen, H.; Rönkkö, T.; Keskinen, J. Comparative Performance of a Thermal Denuder and a Catalytic Stripper in Sampling Laboratory and Marine Exhaust Aerosols. *Aerosol Sci. Technol.* **2018**, *52*, 420–432. [CrossRef]

27. Otsuki, Y.; Tochino, S.; Kondo, K.; Haruta, K. Portable Emissions Measurement System for Solid Particle Number Including Nanoparticles Smaller than 23 nm. *SAE Tech. Pap.* **2017**, *01*, 2402.

28. Yamada, H.; Funato, K.; Sakurai, H. Application of the PMP Methodology to the Measurement of Sub-23nm Solid Particles: Calibration Procedures, Experimental Uncertainties, and Data Correction Methods. *J. Aerosol Sci.* **2015**, *88*, 58–71. [CrossRef]

29. Whelan, I.; Samuel, S.; Hassaneen, A. Investigation into the Role of Catalytic Converters on Tailpipe-Out Nano-Scale Particulate Matter from Gasoline Direct Injection Engine. *SAE Tech. Pap.* **2010**, *01*, 1572.

30. Bogarra, M.; Herreros, J.M.; Hergueta, C.; Tsolakis, A.; York, A.P.E.; Millington, P.J. Influence of Three-Way Catalyst on Gaseous and Particulate Matter Emissions during Gasoline Direct Injection Engine Cold-Start. *Johns. Matthey Technol. Rev.* **2017**, *61*, 329–341. [CrossRef]

31. Dorscheidt, F.; Sterlepper, S.; Görgen, M.; Nijs, M.; Claßen, J.; Yadla, S.K.; Maurer, R.; Pischinger, S.; Krysmon, S.; Abdelkader, A. Gasoline Particulate Filter Characterization Focusing on the Filtration Efficiency of Nano-Particulates down to 10 nm. *SAE Tech. Pap.* **2020**, *01*, 2212.

32. Baek, S.; Jin, D.; Jang, W.; Myung, C.L.; Park, S.; Lee, J. Evaluation of the Time-Resolved Nanoparticle Emissions and the Vehicle Performance Characteristics for a Turbocharged Gasoline Direct-Injection Vehicle with a Metal-Foam Gasoline Particulate Filter. *Proc. Inst. Mech. Eng. Part D J. Automob. Eng.* **2016**, *230*, 745–753. [CrossRef]

33. Johansson, A.; Dahlander, P. Experimental Investigation of the Influence of Boost on Combustion and Particulate Emissions in Optical and Metal SGDI-Engines Operated in Stratified Mode. *SAE Int. J. Engines* **2016**, *9*, 807–818. [CrossRef]

34. Leach, F.; Richard, S.; Richardson, D.; Lewis, A.; Akehurst, S.; Turner, J.; Remmert, S.; Campbell, S.; Cracknell, R. Particulate Emissions from a Highly Boosted Gasoline Direct Injection Engine. *Int. J. Engine Res.* **2018**, *19*, 347–359. [CrossRef]

35. Gong, J.; Viswanathan, S.; Rothamer, D.A.; Foster, D.E.; Rutland, C.J. Dynamic Heterogeneous Multiscale Filtration Model: Probing Micro- and Macroscopic Filtration Characteristics of Gasoline Particulate Filters. *Environ. Sci. Technol.* **2017**, *51*, 11196–11204. [CrossRef]

36. Walter, R.; Neumann, J.; Hinrichsen, O. Extended Model for Filtration in Gasoline Particulate Filters under Practical Driving Conditions. *Environ. Sci. Technol.* **2020**, *54*, 9285–9294. [CrossRef]